THE AMERICAN SOCIETY OF MECHANICAL ENGINEERS
345 E. 47th St., New York, N.Y. 10017

95-GT-1

DISTRIBUTION OF FILM-COOLING EFFECTIVENESS ON A TURBINE ENDWALL MEASURED USING THE AMMONIA AND DIAZO TECHNIQUE

S. Friedrichs, H.P. Hodson and W.N. Dawes
Whittle Laboratory
University of Cambridge
Cambridge, United Kingdom

ABSTRACT

The distribution of adiabatic film-cooling effectiveness on the endwall of a large-scale low-speed linear turbine cascade has been measured using a new technique. This technique is based on an established surface-flow visualisation technique, and makes use of the reaction between ammonia gas and a diazo surface coating. A new method of calibration has been developed to relate the result of the reaction to surface concentration of coolant. Using the analogy that exists between heat and mass transfer the distribution of film-cooling effectiveness can then be determined.

The complete representation of the film-cooling effectiveness distribution provided by the technique reveals the interaction between the coolant ejected from the endwall and the secondary flow in the turbine blade passage. Over- and under-cooled regions on the endwall are identified, illustrating the need to take these interactions into account in the design process. Modifications to the cooling configuration examined in this paper are proposed as a result of the application of the ammonia and diazo technique.

NOMENCLATURE

C	concentration
$I = \frac{\rho_{jet} \cdot V_{jet}^2}{\rho_\infty \cdot V_\infty^2}$	coolant momentum ratio
$M = \frac{\rho_{jet} \cdot V_{jet}}{\rho_\infty \cdot V_\infty}$	coolant blowing ratio
P_0	stagnation pressure
T	temperature
V	velocity
$\dot{m}$	massflow
p	static pressure
η	film-cooling effectiveness
ρ	density
τ	Surface Shear Stress

Subscripts

aw	adiabatic wall (temperature)
iw	impermeable wall (concentration)
jet	coolant jet condition
rel	relative to coolant in plenum [%]
∞	local free stream value

INTRODUCTION

An increase in the cycle efficiency of gas turbines can be achieved through higher turbine entry temperatures. In turn, this requires the development of materials and efficient cooling methods. One cooling method that has gained increasing importance is endwall film-cooling, where coolant air is discharged through discrete holes in the inner and outer endwalls (platforms) of a turbine blade passage. After leaving the holes, the coolant forms a protective layer between the hot mainstream gas and the surface that is to be protected.

The external flow near the endwall, which interacts with the ejected coolant, is three-dimensional due to the presence of secondary flow. A general overview of secondary flow in turbine blade passages is given by Sieverding (1984). Harrison (1989) describes the secondary flow structures in the turbine cascade used in this investigation.

The first work published on endwall film-cooling seems to be by Blair (1974). He found that both heat transfer and film-cooling on the endwall are influenced by secondary flow. A similar observation was made by Takeishi et al. (1989). Their leading edge horseshoe vortex, for example, increased heat transfer and decreased film-cooling effectiveness near the leading edge on the endwall. Granser and Schulenberg (1990) also observed the influence of secondary flow. They ejected coolant from a slot in the endwall upstream of the leading edge and measured higher levels of film-cooling effectiveness near the suction side of the blade than near the pressure side.

Presented at the International Gas Turbine and Aeroengine Congress & Exposition
Houston, Texas - June 5-8, 1995
This paper has been accepted for publication in the Transactions of the ASME
Discussion of it will be accepted at ASME Headquarters until September 30, 1995

Goldman and McLallin (1977) and Sieverding and Wilputte (1980) performed aerodynamic measurements and found a significant effect of endwall film-cooling on the loss and angle distributions downstream of the blade passage, illustrating that endwall coolant ejection influences the passage flow field.

Bourguignon (1985) observed that coolant ejection tends to turn the endwall streamlines towards the inviscid streamlines. In Bourguignon's investigation, endwall film-cooling was effective for up to ten hole diameters downstream of ejection. Both Bourguignon (1985) and Bario et al. (1989) found that ejecting the coolant at an angle to the flow has little effect on the jet trajectory, except in the vicinity of the holes. Despite the strong interactions present in endwall film-cooling, the investigations of Harasgama and Burton (1991) and Jabbari et al. (1994) show that high levels of cooling can be achieved with endwall film-cooling.

In the present study, the effectiveness of a film-cooling configuration is assessed by comparing the temperature T_{aw} that an adiabatic wall would assume under the influence of the ejected coolant, with the one that it would assume without coolant ejection. Since the Mach number in this investigation is small, the uncooled adiabatic wall temperature is approximately equal to the free stream temperature T_∞. The adiabatic wall temperature T_{aw} is usually expressed as a dimensionless temperature, or adiabatic film-cooling effectiveness η, with T_{jet} being the coolant temperature at the exit of the cooling hole.

$$\eta_{aw} = \frac{T_{aw} - T_\infty}{T_{jet} - T_\infty} \tag{1}$$

An isothermal film-cooling effectiveness can be defined based on isothermal wall arguments. This is an alternative to the adiabatic film-cooling effectiveness and is used in temperature based experimental studies with isothermal wall conditions.

Techniques for the experimental determination of adiabatic film-cooling effectiveness can be classed into two groups. In the first group the coolant is ejected at a temperature different from the mainstream and the adiabatic wall temperature is measured directly. Thermocouples, thermochromic liquid crystals or infra-red cameras may be used to measure the surface temperature. In these experiments it is often difficult to achieve an adiabatic wall, so corrections are applied to allow for conduction in the wall. The second group of techniques relies on the analogy that exists between heat and mass transfer. Coolant air at the same temperature as the free stream is seeded with a tracer gas, and surface concentrations of the tracer gas are measured. Analogous to the adiabatic film-cooling effectiveness, an impermeable wall effectiveness based on concentration measurements can be defined:

$$\eta_{iw} = \frac{C_{iw} - C_\infty}{C_{jet} - C_\infty} \tag{2}$$

The conditions for the use of the analogy between heat and mass transfer in film-cooling investigations have been reviewed by Shadid and Eckert (1991). When they are met, the impermeable wall concentration field is similar to the adiabatic wall temperature field and the two effectiveness parameters are equal:

$$\eta_{iw} = \eta_{aw} \tag{3}$$

This is the case in typical film-cooling investigations, where Reynolds numbers are high and turbulent mixing dominates over molecular diffusion. Molecular parameters such as Prandtl and Schmidt numbers have very little influence. The results of Pedersen et al. (1977), for example, illustrate that the impermeable wall effectiveness is practically independent of the Schmidt number over their investigated range. Therefore the C_{iw} distribution in a concentration based film-cooling experiment will be representative of the T_{aw} distribution of a temperature based experiment having similar Reynolds numbers and coolant to free stream property ratios.

To date, surface concentration measurements have been performed by analysing gas samples taken either through tappings in the wall or through probes or rakes adjacent to the surface. This paper describes an alternative technique for performing surface concentration measurements; the ammonia and diazo surface coating technique.

In both the temperature and concentration based experiments, different techniques are capable of different degrees of resolution of film-cooling effectiveness. Jabbari et al. (1994), for example, encountered difficulties with their gas sampling technique. The coolant trajectories moved relative to the fixed gas sampling tappings as experimental conditions were varied. In practice, thermocouple techniques and techniques based on sampling gas through wall tappings are only able to measure at predetermined locations. Probe sampling techniques, thermochromic liquid crystal, infra-red camera or ammonia and diazo techniques cover a large area of the surface and provide a complete representation of the film-cooling effectiveness.

THE AMMONIA AND DIAZO TECHNIQUE

The use of the ammonia and diazo surface coating technique for measuring adiabatic film-cooling effectiveness is based on an established surface-flow visualisation technique. In investigations such as those reported by Joslyn and Dring (1983) and Hodson and Addison (1989), the surface of the test piece is covered with diazo coated paper. Pure ammonia gas is then either passed slowly through wall tappings or is ejected from an upstream probe. The ammonia gas reacts with the diazo coating, leaving a trace on the paper as it is transported over the surface by the flow under investigation. Dring et al. (1980) and Jabbari et al. (1994) used the same basic technique to visualise coolant flow in film-cooling investigations. The coolant air was seeded with ammonia gas and was passed over a surface covered with diazo paper, leaving traces of varying darkness.

The first suggestion of the use of the ammonia and diazo technique for quantitative effectiveness measurements seems to have been by Soechting et al. (1987). To simulate a realistic density ratio they used CO_2 as coolant, demonstrating the use of the basic technique with coolant gases other than air. They did not develop a quantitative ammonia and diazo technique, as they concluded that extensive calibrations were necessary to correlate the darkness of the trace to the coolant concentration.

The method of calibration described below was developed to allow the calculation of film-cooling effectiveness from the

measured darkness. A detailed description of this new method of calibration and of the use and validation of the ammonia and diazo surface coating technique for the measurement of adiabatic film-cooling effectiveness is given in Friedrichs and Hodson (1994).

The Diazo Surface Coating

The chemicals of the diazo surface coating are usually applied to paper or polyester film, which is then fixed to the experimental surface. In the experiments presented here, a polyester film with a thickness of 0.05 mm was used. The film is covered with the chemicals embedded in a resin. The use of film was preferred over the use of paper as it has a smoother surface and is easier to remove from the test piece after being fixed with low-tack double-sided tape. In the study of very complex three-dimensional geometries where paper or film cannot be fixed satisfactorily, they may however be applied directly to the surface.

The mixture of chemicals usually consists of ten to fifteen different components, mainly diazos, couplers, and additives. The diazos are light sensitive and react with ammonia and water to form radicals. Exposure to light desensitises the diazos to ammonia and water. The couplers react with the radicals to form the dyes that darken the surface coating. The additives may include stabilisers, contrast enhancers and ethylene glycol to absorb moisture.

Experimental Procedure and Processing

The measurement technique relies on the principle that the darkness of the traces on the diazo surface coating is dependent on the surface concentration of the ammonia and water vapour in the coolant gas. Prior to the experiment, diazo film is fixed to the experimental surface. The wind tunnel is started and conditions are allowed to stabilise. The cooling air is then seeded with ammonia gas and water vapour. In the experiments presented here, the average ammonia concentration was ~0.5%, the average relative humidity was ~90%, and the exposure time was between one and two minutes. These values can be varied to achieve the desired darkness of the traces, as long as both ammonia and water vapour are present for the chemical reaction to take place. After the experiment, the image is fixed by exposure to light to prevent further reaction. An example of the resulting traces on a flat plate is shown in Fig. 1.

Fig. 1: Coolant Traces on a Diazo Coated Flat Plate

A visual inspection of Fig. 1 directly reveals coolant trajectories, but to determine cooling effectiveness the relationship between the darkness of the trace and the surface concentration of coolant has to be found. The reaction between the diazo surface coating and the coolant seeded with ammonia gas and water vapour is dependent on a variety of factors. Increases in ammonia concentration, humidity, and exposure time each result in a darker image. An increase in temperature results in a lighter image, with a temperature difference of merely 3°C resulting a change in relative darkness of about 20%.

To avoid individual calibrations for each of these dependencies, a reference experiment is performed parallel to the main experiment. In the reference experiment, a calibration strip such as the one shown in Fig. 2 is produced by mixing the coolant gas mixture with free stream air from the wind tunnel in known ratios. All the above dependencies are automatically taken into account, as the calibration strip is exposed to representative mixtures for the same amount of time as the main experiment.

0% 10% 20% 30% 40% 50% 60% 70% 80% 90% 100%

Relative Concentration C_{rel} [%]

Fig. 2: Calibration Strip Produced for the Trace in Fig. 1

To create this calibration strip, a mixing box has been designed (see Fig. 3). It provides eleven sampling tubes with coolant to mainstream mixtures of 0% to 100%, in 10% steps. Each of the sampling tubes is fed by a total of ten holes. The 0% tube is fed from ten holes ejecting mainstream air, the 10% tube is fed from nine mainstream holes and one coolant gas hole, and so on. The air in each of the sampling tubes is passed over a strip of diazo paper or film, creating the calibration strip. The design concentrations in the sampling tubes are achieved with uniform flowrates through all of the holes. The design criteria for the mixing box therefore were uniform hole shapes and diameters, sufficiently large plenum chambers, uniform exit static pressures and equal pressures in the two plenum chambers. The completed mixing box was calibrated by analysing gas samples from each of the sampling tubes, and was found to function as designed.

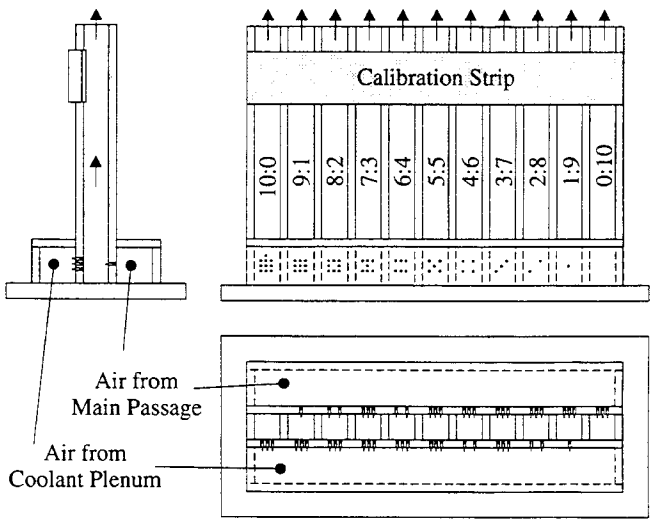

Fig. 3: Mixing Box for On-Line Calibration

In order to quantify the darkness distribution obtained using the ammonia and diazo technique, both the image and the corresponding calibration strip are digitised simultaneously using an optical scanner. The analysis of the calibration strip gives the relationship between the darkness of the trace and the relative concentration of the coolant. This results in calibration curves such as the one shown in Fig. 4. By applying the calibration using interpolation between the calibration points, the relative concentration of each measurement point is determined.

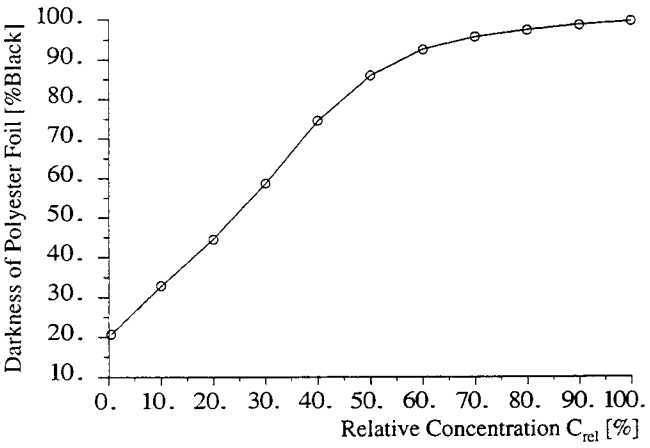

Fig. 4: Calibration Curve Derived from Strip in Fig. 2

In the present experiments only the coolant is seeded with ammonia and water vapour. The free stream concentration therefore corresponds to a value of 0%. With the relative coolant concentration in the plenum being 100%, the measured relative concentration values are equivalent to the adiabatic film-cooling effectiveness. Equations (2) and (3) therefore become:

$$\eta_{aw} = \eta_{iw} = \frac{C_{iw}}{C_{jet}} = C_{rel} \qquad (4)$$

Validation and Discussion

To validate the ammonia and diazo technique, Friedrichs and Hodson (1994) compared cooling effectiveness data obtained using the ammonia and diazo technique with data obtained using a gas sampling technique. This comparison was performed for a flat plate with a single row of five discrete film-cooling holes. The five holes had a hole length to diameter ratio of 3.5, a spacing to diameter ratio of 3.0 and were inclined at an angle of 35° to the surface in direction of the free stream. The experiments were run at low speed, unity density ratio, and a blowing ratio M = 0.5.

Fig. 1 shows the coolant trace downstream of the central hole, with traces from neighbouring holes visible on either side. In the gas sampling technique, the cooling air was seeded with ethylene gas and samples were taken from surface tappings at fixed locations downstream of the central hole. Using an infra-red gas-analyser, the concentration of the tracer gas in the samples of the surface flow was determined. Fig. 5 shows the comparison between the results of the gas sampling technique and averaged results from the ammonia and diazo technique. The 'spikes' in the ammonia and diazo results are due to holes in the polyester film at the locations of the gas sampling tappings. The comparison shows that the results are in good agreement.

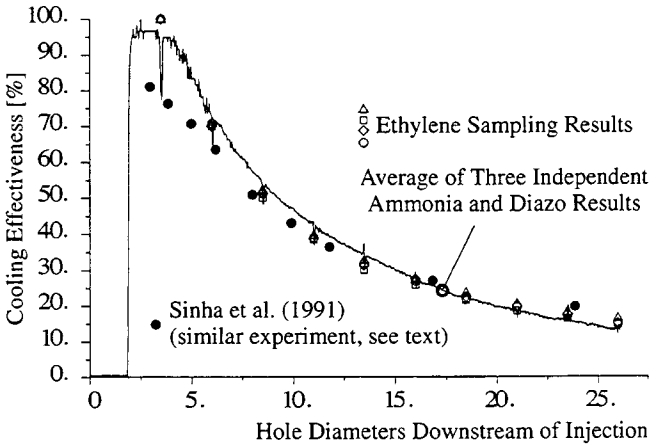

Fig. 5: Centreline Cooling Effectiveness Data Obtained Using Two Measurement Techniques (Friedrichs and Hodson (1994)) Comparison to a Similar Experiment by Sinha et al. (1991)

Included in Fig. 5 are results from Sinha et al. (1991). They measured centreline cooling effectiveness in a similar experiment using a temperature based measurement technique. Their experiment differed from the present one in the coolant to mainstream density ratio (1.2 vs. 1.0), the coolant hole length to diameter ratio (1.75 vs. 3.5), and possibly the inlet boundary layer which was not measured in the present experiment.

Agreement between the results is good, except in the vicinity of the hole where gradients are high. The difference in density ratio is unlikely to be the cause of the discrepancy, as Sinha et al. (1991) showed that density ratio has no noticeable effect at this low blowing ratio. Schmidt et al. (1994) showed that the same is true for the length to diameter ratio. Although not measured, the boundary layer is expected to be similar to the one found in the experiments of Sinha et al. (1991). According to Bogard (1995), the discrepancy may be due to conduction problems with the thermal measurements, illustrating a possible limitation of thermal techniques.

The calibration curve shown in Fig. 4 is similar to the curves used in obtaining the results in Fig. 5. It illustrates the non-linearity of the relationship between darkness and concentration. For these experiments, saturation is reached above 60%...70% coolant concentration. The resolution in that region is significantly reduced. A small change in measured darkness results in a large change in interpreted coolant concentration. The large steps in the regions of high cooling effectiveness of the ammonia and diazo results in Fig. 5 illustrate this effect.

Both the validation experiment and the endwall film-cooling experiment described here were conditioned to give good resolution at low levels of cooling effectiveness. They are therefore well suited to determine the overall distribution of cooling effectiveness. If lighter traces are produced, for example through lower concentrations of ammonia, the experiment can be conditioned to give good resolution at high levels of cooling

effectiveness. Details in regions of high cooling effectiveness, for example in the vicinity of coolant jets, can then be studied.

Experiments were performed in two different facilities to determine if the flow Reynolds number or if ammonia or water vapour depletion have an influence on the darkness of the trace. For the depletion experiment, a mixture of ammonia and water vapour was passed through a two metre long tube, the inside of which was coated with diazo film. For the Reynolds number experiment, a mixture of fixed concentration was passed over a series of diazo film strips at different flow velocities, covering the range of Reynolds number found in the experiment. Neither the Reynolds number nor ammonia or water vapour depletion had a detectable effect on the darkness.

Sometimes it may not be possible to produce a valid calibration strip such as the one shown in Fig. 2. This may happen when the mixing box and its feed lines are not adiabatic, and the coolant, mainstream and mixing box temperatures differ. An alternative method of calibration is proposed by Haslinger and Hennecke (1994). For a specific experimental condition, a gas sampling technique such as the one used by Jabbari et al. (1994) may be used to determine concentrations at discrete locations on the surface. An ammonia and diazo trace is produced for the same condition. By comparing the measured surface concentrations to the darkness values of the trace at the same locations, a calibration curve can be derived. By using this alternative method of calibration the dependencies of the ammonia and diazo reaction are also taken account of, and the advantages inherent in the ammonia and diazo technique remain.

TURBINE CASCADE AND COOLING CONFIGURATION

The endwall film-cooling investigation presented here was performed on a large-scale, low-speed, linear turbine cascade. The cascade consists of four blades with a true chord of 278 mm, a span of 300 mm, and a pitch of 230 mm. The flow enters the cascade at an angle of 40° and is turned through 105°. With the low aspect ratio and high turning angle, the blades produce strong secondary flows. These are stronger than the ones found in high pressure nozzle guide vanes with a typical turning angle of 70°, and therefore allow a more detailed observation of the basic interactions between endwall coolant ejection and the passage flow field. Details of the basic cascade without endwall film-cooling can be found in Harrison (1989).

Fig. 6 shows oil and dye surface-flow visualisation on the cascade endwall without coolant ejection. The three-dimensional separation lines can clearly be seen. For ease of comparison, they are also shown in Fig. 7 and Fig. 8 as dashed lines.

Coolant air is ejected from a common plenum chamber through 43 holes in one endwall of a single passage. Fig. 7 shows the cooling configuration that consists of four single rows of holes and four individual holes, all having a diameter of 4 mm and ejecting at an angle of 30° to the surface. The thickness of the endwall is 12 mm, giving a length to diameter ratio of 6, typical of endwall film-cooling configurations.

This cooling configuration would provide cooling to most of the endwall surface in the absence of secondary flow. It is therefore well suited to investigate the effect that the interactions between the ejected coolant and the endwall flow field have on

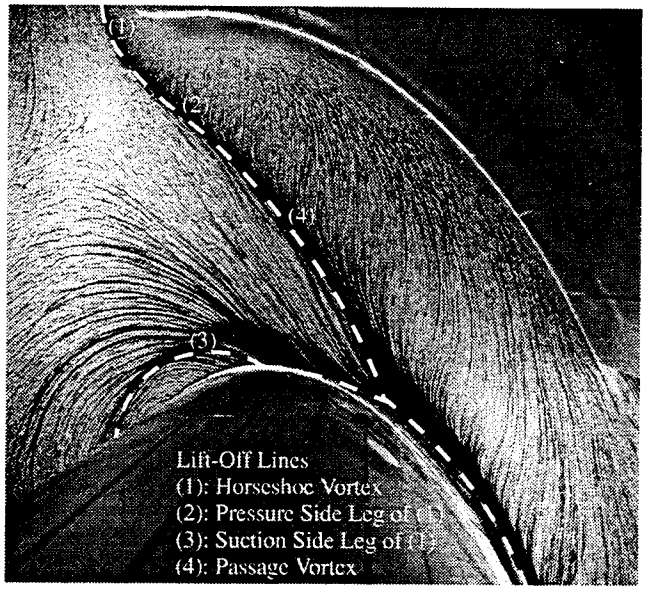

Fig. 6: Oil and Dye Surface-Flow Visualisation on the Cascade Endwall Without Film-Cooling

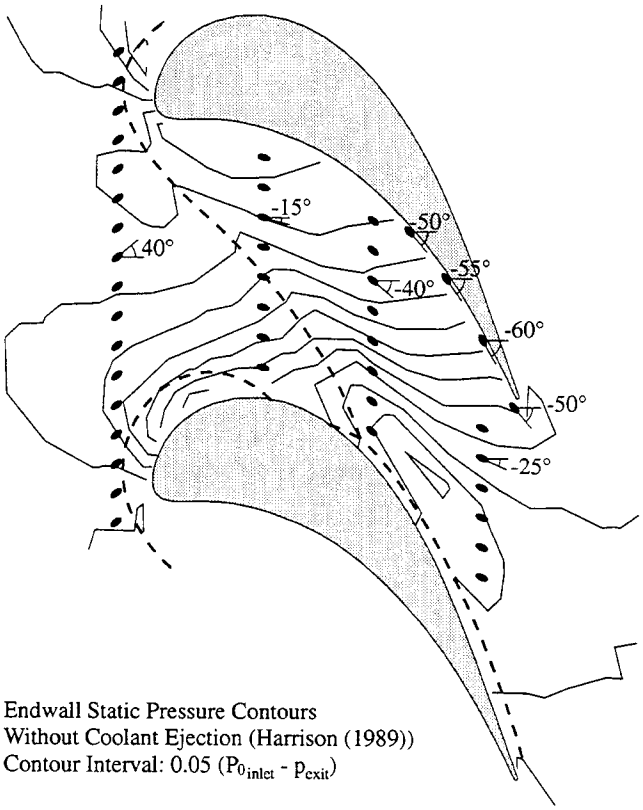

Fig. 7: Cascade Endwall with Film-Cooling Holes, Endwall Static Pressure Contours and Lift-Off Lines Without Film-Cooling

the distribution of film-cooling effectiveness. The first row of holes is located upstream of the leading edge, ejecting in the inlet

flow direction. The second row of holes is located at 30% axial chord and ejects in approximately the inviscid streamline direction. The third row is at 60% axial chord, again ejecting in approximately the inviscid flow direction. The fourth row at 90% axial chord ejects at an angle to both the inviscid and the actual endwall flow.

The single holes near the blade pressure surface were designed to provide internal cooling. The air is intended to convectively cool the metal of the endwall as it passes through the holes. Upon reaching the surface it is ejected and used for film-cooling purposes. Three of the single holes are located in the corner between the pressure surface of the blade and the endwall in the second half of the blade passage. They eject in the flow direction. The fourth single hole is located just downstream of the trailing edge, and is angled to the flow in an attempt to direct coolant into the wake of the trailing edge.

Each of the cooling holes experiences a different exit static pressure as it ejects into the flow field near the endwall. The undisturbed endwall static pressure field as measured by Harrison (1989) is also shown in Fig. 7. Coolant ejection will locally affect the pressure field in the vicinity of the holes due to the blockage presented by the jet. Due to its interaction with the passage flow field, coolant ejection will also influence the overall passage pressure field. In a first approximation the undisturbed pressure field is used to determine the local hole exit static pressures.

Fig. 8 shows the distribution of the mean shear stress coefficient on the endwall. It was calculated by Harrison (1989) from surface shear stress measurements obtained using the oil drop method. Using the Reynolds analogy, this distribution can be viewed as a distribution of Stanton number. From it, one can see that the region downstream of the lift-off line in the first half of the blade passage is one of potentially high heat transfer. Towards the rear of the blade passage the values fall, leaving a local peak where the three-dimensional separation lines reach the blade suction surface. Flow velocities are high in the rear part of the blade passage, especially near the blade suction surface (see Fig. 7). As heat transfer coefficients are proportional to Stanton number multiplied by velocity, this also is a region of potentially high heat transfer.

TEST CONDITIONS

In the present experiment, air is supplied to the common plenum chamber at the same temperature as the free stream. As density changes due to the tracer amounts of ammonia gas and water vapour are negligible, this results in a unity coolant to free stream density ratio. For the experimental conditions presented here, the coolant plenum pressure equals the inlet stagnation pressure. The ratio of coolant exit velocity to local free stream velocity is therefore approximately equal for all holes.

An isentropic coolant massflow was calculated based on the experimental conditions, hole diameters and measured hole exit static pressures. It was compared to the coolant massflow measured during the experiment. The comparison gave an average reduction in massflow by a factor of 0.67. The reduction is caused by flow separation off the inlets of the coolant holes. The separation creates three-dimensional flow structures with counter-

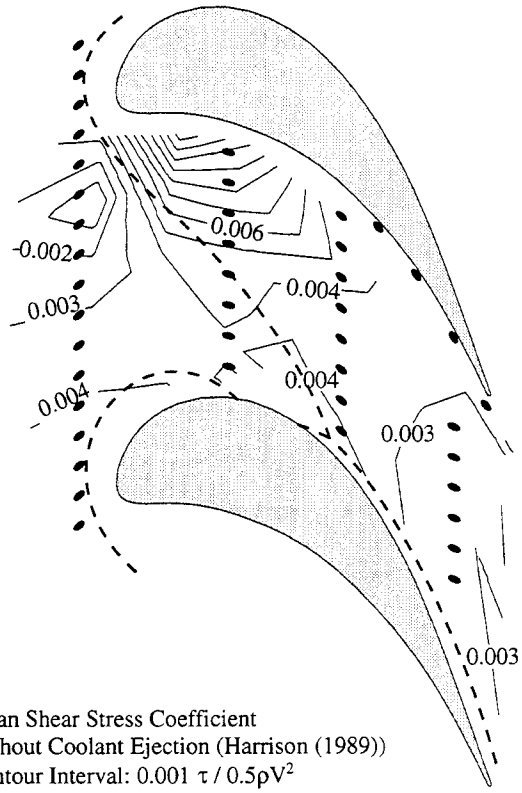

Fig. 8: Distribution of Mean Shear Stress Coefficient on the Endwall Without Film-Cooling

rotating vortices and large velocity gradients, as can be seen in the computational predictions of Leylek and Zerkle (1993). As a result, all coolant holes operate with a blowing ratio of $M \approx 0.67$ and a momentum ratio of $I \approx 0.45$.

For the passage under investigation, the total coolant massflow was equivalent to 1.64 % of the passage massflow, if both endwalls had been cooled. The distribution of the coolant massflow for the passage is shown in Table 1.

configuration	% of total coolant flow	
row of holes upstream of leading edge	26.6 %	13 holes
row of holes at 30% axial chord	17.3 %	8 holes
row of holes at 60% axial chord	22.5 %	8 holes
row of holes at 90% axial chord	23.4 %	6 holes
single holes	10.2 %	4 holes

Table 1: Distribution of the Coolant Massflow in a Single Passage

The results presented in this paper were produced with the cascade operating at a Reynolds number of 8.6×10^5 based on exit velocity and true chord, which corresponds to a Reynolds number of 4.5×10^5 based on inlet velocity and true chord. Harrison (1989) measured the inlet boundary layer at a point half an axial chord upstream of the leading edge and found it to have a thickness of 18 mm, a displacement thickness of 2.6 mm, a momentum

thickness of 1.9 mm and a shape factor of 1.36. The inlet turbulence level of the free stream was of the order of 0.5%.

DISCUSSION OF RESULTS

The distribution of cooling effectiveness on the cascade endwall was measured using the ammonia and diazo technique. Two A4 sheets of polyester film were required to cover the relevant regions of the endwall. The traces left by the coolant which had been seeded with ammonia and water vapour are shown in Fig. 9.

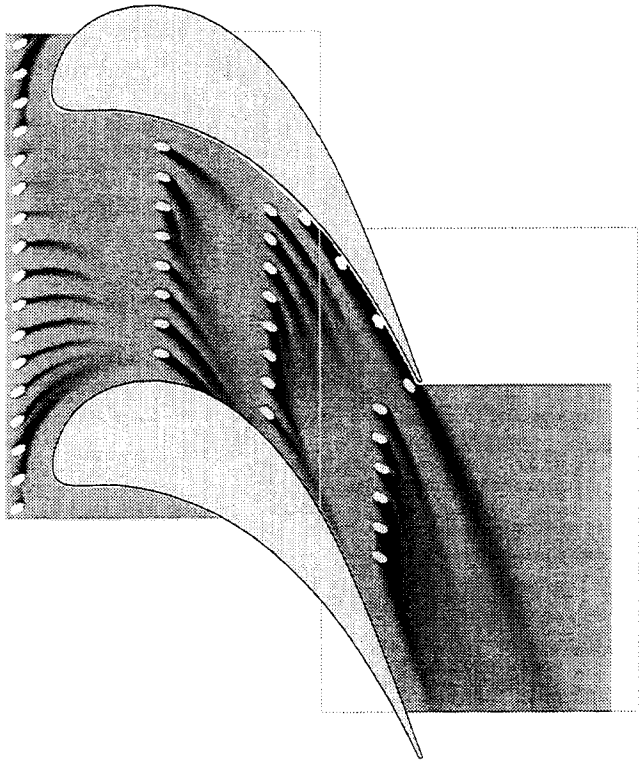

Fig. 9: Traces on the Surface Coating of the Turbine Endwall

The darkness distribution on each of the sheets was scanned together with the calibration strip produced during this experiment. Darkness values were measured out of a range of 256 greyscales at a resolution of 75 dots per inch, giving approximately 3 measurement points per millimetre. After processing, the film-cooling effectiveness results from the two sheets were combined in Fig. 11. A comparison of the results in Fig. 11 with the joint between the two sheets of film seen in Fig. 9 shows continuous contours across the joint, illustrating that possible differences between sheets of film or in scanning and processing are negligible.

Fig. 10 shows an oil and dye visualisation of the endwall surface-flow under the influence of the ejected coolant. Due to the blockage presented by the leading edge, the incoming endwall boundary layer is subjected to a stagnating pressure gradient. This causes the boundary layer to undergo three-dimensional separation and to roll up into a horseshoe vortex. The legs of the horseshoe vortex pass to either side of the blade. The suction-side leg travels around the blade and its lift-off line later intersects the blade suction surface. The pressure side leg moves into the blade passage and merges with the main passage vortex. The passage vortex moves across to the suction surface of the neighbouring blade under the influence of the passage pressure field. The incoming boundary layer separates along the lift-off line of the passage vortex. Downstream of the lift-off line, Harrison (1989) found the new boundary layer to be thin, highly skewed, and largely laminar.

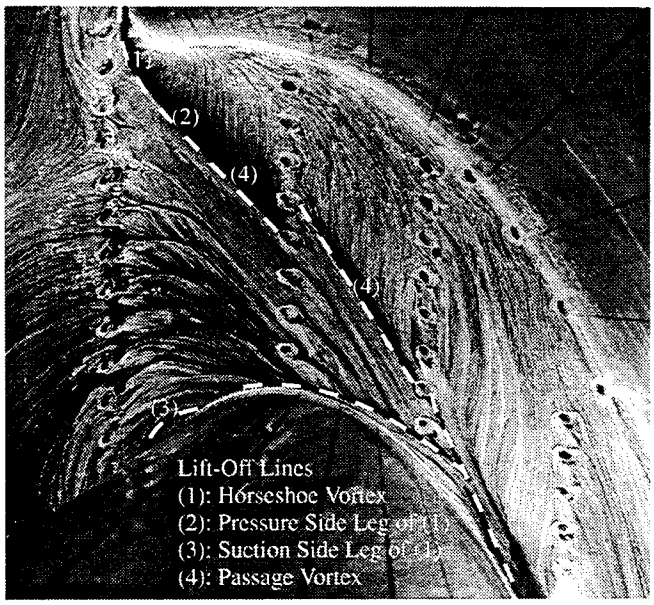

Fig. 10: Oil and Dye Surface-Flow Visualisation on the Film-Cooled Cascade Endwall

A comparison to the case without coolant ejection (see Fig. 6 and Fig. 7), shows that the lift-off line of the horseshoe vortex has moved closer to the leading edge. A similar observation is made by taking the two coolant holes at 60% axial chord near the blade suction surface as a reference, and comparing the locations of the lift-off line with and without coolant ejection (see Fig. 7 and Fig. 10). The comparison reveals that the lift-off line of the passage vortex has moved downstream. In both cases the ejection of coolant seems to have delayed the separation of the inlet boundary layer. The most visible influence of the ejected coolant on the secondary flow can be seen at the row of holes at 30% axial chord. The three-dimensional separation of the inlet boundary layer is delayed due to the coolant ejection, resulting in a displacement of the lift-off line. The three-dimensional separation lines shown in Fig. 10 are also shown as dashed lines in Fig. 11 to simplify comparisons.

The Row of Holes Upstream of the Leading Edge

Takeishi et al. (1989) found that the leading edge horseshoe vortex increased heat transfer and decreased cooling effectiveness near the leading edge. In this investigation, Fig. 11 shows that the horseshoe vortex prevents coolant from being effective in the area

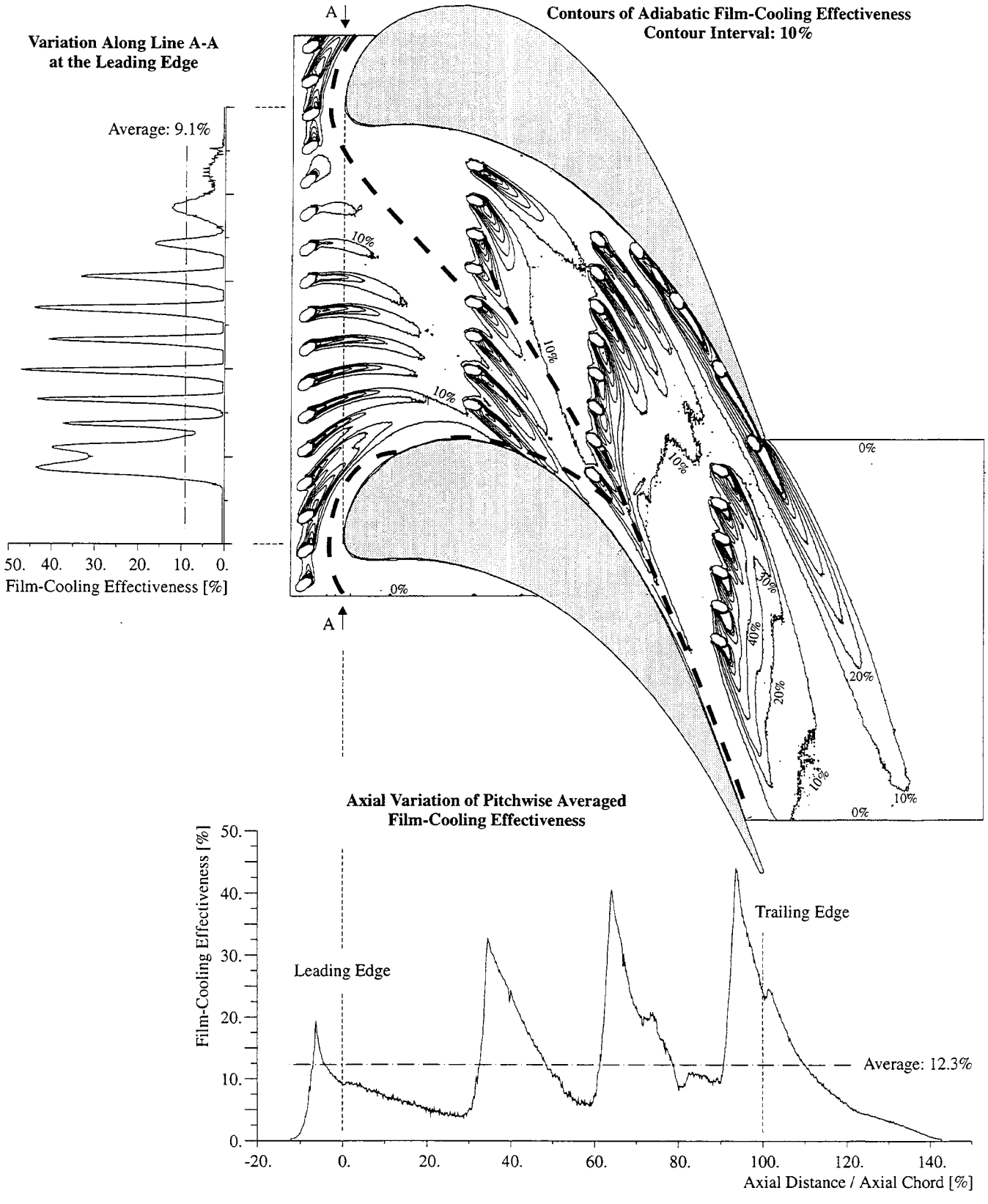

Fig. 11: Endwall Film-Cooling Effectiveness Measured Using the Ammonia and Diazo Technique

between its lift-off line and the blade. This area of high heat transfer is therefore virtually unprotected, even with jets aimed directly at the blade leading edge. A possible solution to this problem is to place cooling holes downstream of the lift-off line of the horseshoe vortex, into the corner of the blade with the endwall.

The holes at the leading edge eject coolant into the inlet boundary layer before it separates. Fig. 11 shows that cooling is present in the region downstream of the holes and upstream of the lift-off lines, although the levels of cooling effectiveness are not as high as the ones found towards the rear of the passage. The coolant trajectories near the blade suction surface in the mouth of the blade passage display little lateral spreading and high persistence. This indicates reduced mixing, probably due to accelerating flow in this region. Cooling is provided almost up to the row of holes at 30% axial chord. An uncooled area remains between the pressure surface of the blade, the lift-off lines, and the cooling holes at 30% axial chord. This is unfortunate, as Fig. 8 indicates high levels of Stanton number in this region. Takeishi et al. (1989) and Gaugler and Russell (1983) also measured high heat transfer in this area. The addition of cooling holes in this region is again a possible solution to the problem.

Included in Fig. 11 is the local variation of effectiveness along the leading edge. It shows that even though there are significant gaps between the traces of coolant jets, the integrated average cooling effectiveness is 9.1%. The axial variation of pitchwise averages can also be seen in Fig. 11. It shows that average effectiveness upstream of the row of holes at 30% axial chord is lower than the endwall average of 12.3%, reflecting the large uncooled area near the pressure surface.

The Row of Holes at 30% Axial Chord

The holes at 30% axial chord eject into two different regions of flow which are divided by the path of the passage vortex. The holes near the blade suction surface are upstream of the lift-off line of the passage vortex. They eject into the inlet boundary layer that is thickened as it is 'funnelled' into the region having the suction side leg of the horseshoe vortex on one side and the passage vortex on the other. The influence of this 'funnelling' can be seen in Fig. 11. The trajectories of the affected jets merge and create a blanket of cooling without uncooled gaps. This is beneficial, as heat transfer in this region can be high. Fig. 8 suggests a local peak in Stanton number in this region, which combined with high velocities would result in high heat transfer. The comparison between endwall heat transfer and secondary flow given by Gaugler and Russell (1983), also shows a local peak in heat transfer where the three-dimensional separation lines reach the suction surface.

The holes near the blade pressure surface are downstream of the lift-off line of the passage vortex. They eject into the new, thin endwall boundary layer. Fig. 11 shows that the trajectory of the coolant from the hole nearest to the pressure surface approximately follows the inviscid streamline direction, leaving an uncooled gap in the blade-endwall corner. A comparison with the surface-flow visualisation in Fig. 10 shows that the endwall flow in the trajectory of this jet diverges. This seems to have a positive influence, as both the lateral spreading and the persistence of this trajectory are high. Of all the holes in the endwall, this is the hole that experiences the highest exit static pressure. It therefore has the lowest coolant massflow. The hole next to the suction surface in the same row of holes has approximately three times the massflow. Considering the low massflow, the cooling performance from this hole is very good. However, if the pressure in the plenum is lowered sufficiently, it will be the first hole to experience reverse flow.

The influence of secondary flow is visible in Fig. 11 in the trajectories coming from the second and third holes from the pressure surface. They are turned towards the suction surface as the jets mix out. The fourth hole is located in the vicinity of the lift-off line of the passage vortex. The separation of the inlet boundary layer and the resulting upwash cause the jet to lift off the endwall before it is able to provide much cooling.

Fig. 11 shows that due to the strong deflection of the trajectories an area with hardly any cooling is formed upstream of the row of holes at 60% axial chord. Fig. 8 again shows the uncooled region to be one of potentially high heat transfer. Additional holes are needed to provide cooling in this area, as the new, thin endwall boundary layer downstream of the lift-off line enhances heat transfer to the endwall.

The axial variation of pitchwise averaged cooling effectiveness in Fig. 11 shows that the row of holes at 30% axial chord performs better than the row upstream of the leading edge. Most of the region between 30% and 60% axial chord displays an average film-cooling effectiveness higher than the endwall average. Again, the effect of the uncooled region upstream of the next row of holes is clearly seen.

The Row of Holes at 60% Axial Chord

The interaction of the secondary flow with the coolant jets coming from the row of holes at 60% axial chord is similar to the one found at 30% axial chord. Fig. 11 shows that near the pressure surface, jet trajectories are in approximately the inviscid streamline direction. The traces merge at a low level of cooling effectiveness, but retain individual high effectiveness regions downstream of the holes. Towards the middle of the blade passage there again is an influence of secondary flow. The jet trajectories are short and turned towards the suction surface. The coolant leaves the endwall to be entrained into the passage vortex before providing much cooling. The hole nearest to the suction surface provides cooling for a long distance downstream of ejection. Some of its coolant may be entrained in a vortex that forms in the corner of the suction surface of the blade with the endwall, as the endwall cross-flow starts to move up the suction surface. Again a large, triangular area upstream of the next row of holes remains practically uncooled due to the influence of secondary flow. Stanton numbers inferred from Fig. 8 are low in this region, but velocities are high (see Fig. 7) and high rates of heat transfer are to be expected. The cooling holes near the lift-off line that are not effective would be better placed in this region.

The pitchwise averages of cooling effectiveness in Fig. 11 show that the effectiveness in the vicinity of the holes at 60% axial chord is higher than the one for the row upstream. As the jets mix out, the high effectiveness traces from the single holes in the pressure surface- endwall corner cause a rise in the averages,

and keep them from falling below ~10%. This masks the effect of the large uncooled area upstream of the row of holes at 90% axial chord.

The Row of Holes at 90% Axial Chord

The holes discussed up to now have been ejecting coolant in approximately the inviscid streamline direction. The holes at 90% axial chord eject at an angle to this direction, resulting in a large ejection angle to the endwall cross-flow. Fig. 11 shows that the exit angle is not the direction of the coolant trajectories. The coolant is turned towards the suction surface as soon as it leaves the holes. This corresponds to the findings of Bourguignon (1985) and Bario et al. (1989), who found that ejecting the coolant at an angle to the flow has little effect on the jet trajectory, except in the vicinity of the holes. Although the effect on trajectories is small, there is a large effect on the endwall flow. A comparison of Fig. 10 with Fig. 6 shows that the endwall cross-flow has been reduced. The difference in endwall flow angle upstream and downstream of the holes is large, and the amount of overturning near the endwall is reduced.

Fig. 11 shows that the coolant jets at 90% axial chord merge, forming an insulating layer of coolant that is effective for a large distance downstream of ejection. The regions to either side of this blanket remain uncooled. As these areas lie in regions of potentially high heat transfer, additional holes closer to the blade surfaces are necessary to close the gaps.

Pressure Surface - Endwall Corner

The three single holes in the corner of the blade pressure surface with the endwall eject into the inviscid streamline direction, and the trajectories are oriented accordingly. The lateral spreading of the trajectories is enhanced as the endwall cross-flow develops, but not sufficiently so to transport the coolant across the blade passage. The cooling effectiveness is high, and in the context of endwall film-cooling fewer holes would have sufficed.

The cooling effectiveness downstream of the single hole at the trailing edge greatly benefits from the amount of coolant present in the upstream corner. It is angled in an attempt to cool the endwall in the wake of the trailing edge. As this is a region of high levels of turbulence and vortical motion, it was initially expected that providing film-cooling would be difficult. Assisted by the holes in the pressure surface corner, the coolant ejected from the hole at the trailing edge gives high levels of effectiveness, has a high degree of lateral spreading and is effective for a very long distance downstream of ejection.

CONCLUSIONS

The ammonia and diazo surface coating technique has been developed and successfully used to measure the distribution of adiabatic film-cooling effectiveness on the endwall of a large-scale, low-speed, linear turbine cascade. The cooling effectiveness distribution was presented together with surface-flow visualisation, revealing the strong interactions between endwall coolant ejection and secondary flow in the blade passage. The turbine cascade was designed to produce very strong secondary flow; stronger than would be found in most engine nozzle guide vanes. This exaggerates the effects, but aids in the illustration and understanding of the basic flow interactions.

The results presented here have shown that the flow structures associated with the three-dimensional separation lines on the endwall can act as barriers to the coolant trajectories on the surface. Coolant ejection underneath the lift-off lines is inefficient, as most of the coolant leaves the surface before providing much cooling. Coolant ejected away from the lift-off lines can provide cooling to a larger area. Ejection near the blade pressure surface into the diverging endwall cross-flow is efficient, as it gives traces with a high degree of lateral spreading and penetration. The trajectories of the coolant were not found to be determined by the angle of ejection to the flow, except in the vicinity of the holes.

The endwall surface-flow field has been modified by coolant ejection. The lift-off lines have moved downstream as the ejection of coolant delayed the three-dimensional separation of the inlet boundary layer. The amount of overturning near the endwall downstream of the cascade was reduced, with the endwall cross-flow being turned towards the inviscid streamlines.

The tested cooling configuration did not provide a complete coolant coverage of the endwall. Nonetheless, the area averaged cooling effectiveness for the endwall was found to be 12.3%. The uncooled areas have been identified, and modifications to the configuration have been proposed.

In endwall film-cooling studies it is necessary to measure the complete distribution of film-cooling effectiveness or heat transfer. This allows insight into the flow interactions and quickly identifies over- and under-cooled regions. With the ammonia and diazo surface coating technique, a technique for measuring adiabatic film-cooling effectiveness has been developed that not only gives the complete distribution, but is also easy to use, fast, and low-cost.

ACKNOWLEDGEMENTS

The authors are grateful for the support provided by Rolls-Royce plc, the Engineering & Physical Sciences Research Council (EPSRC), and the Frankfurt Main Flughafen Stiftung (Frankfurt Airport Foundation). They would also like to thank Ozalid (UK) Ltd., especially Mr. Faiers, for valuable technical advice and for providing Ozalid paper and Ozafilm samples, Prof. Denton for the use of the cascade, the technical staff of the Whittle Laboratory, especially Mr. Saunders, for their assistance, and Prof. Hennecke and Dipl.-Ing. Haslinger in Darmstadt for their useful discussions concerning the measurement technique.

REFERENCES

Bario, F., Leboeuf, F., Onvani, A., and Seddini, A., 1989, "Aerodynamics of Cooling Jets Introduced in the Secondary Flow of a Low Speed Turbine Cascade", ASME Paper 89-GT-192

Blair, M.F., 1974, "An Experimental Study of Heat Transfer and Film Cooling on Large-Scale Turbine Endwalls", ASME *Journal of Heat Transfer*, Vol. 96, pp. 524-529

Bogard, D.G., 1995, Private Communications, University of Texas at Austin, USA

Bourguignon, A.E., 1985, "Etudes des Transferts Thermiques sur les Plates-Formes de Distributeur de Turbine avec et sans Film de Refroidissement", AGARD-CP-390, *Heat Transfer and Cooling in Gas Turbines*

Dring, R.P., Blair, M.F., and Joslyn, H.D., 1980, "An Experimental Investigation of Film Cooling on a Turbine Rotor Blade", ASME *Journal of Engineering for Power*, Vol. 102, pp. 81-87

Friedrichs, S. and Hodson, H.P., 1994, "The Ammonia and Diazo Surface Coating Technique for Measuring Adiabatic Film Cooling Effectiveness", *12th Symposium on Measuring Techniques for Transonic and Supersonic Flow in Cascades and Turbomachines,* Prague, The Czech Republic

Goldman, L.J. and McLallin, K.L., 1977, "Effect of Endwall Cooling on Secondary Flows in Turbine Stator Vanes", AGARD-CPP-214

Granser, D. and Schulenberg, T., 1990, "Prediction and Measurement of Film Cooling Effectiveness for a First-Stage Turbine Vane Shroud", ASME Paper 90-GT-95

Gaugler, R.E. and Russell, L.M., 1983, "Comparison of Visualised Turbine Endwall Secondary Flows and Measured Heat Transfer Patterns, ASME Paper 83-GT-83

Harasgama, S.P. and Burton, C.D., 1991, "Film Cooling Research on the Endwall of a Turbine Nozzle Guide Vane in a Short Duration Annular Cascade, Part 1: Experimental Technique and Results", ASME Paper 91-GT-252

Harrison, S., 1989, "The Influence of Blade Stacking on Turbine Losses", Ph.D. Thesis, University of Cambridge; see also Harrison, S., 1989, "Secondary Loss Generation in a Linear Cascade of High-Turning Turbine Blades, ASME Paper 89-GT-47

Haslinger, W., and Hennecke, D.K., 1994, Private Communications, Technische Hochschule Darmstadt, Germany

Hodson, H.P. and Addison, J.S., 1989, "Wake-Boundary Layer Interactions in an Axial Flow Turbine Rotor at Off-Design Conditions", ASME *Journal of Turbomachinery*, Vol. 111, No. 2, pp 181-192

Jabbari, M.Y., Marston, K.C., Eckert, E.R.G., and Goldstein, R.J., 1994, "Film Cooling of the Gas Turbine Endwall by Discrete-Hole Injection", ASME Paper 94-GT-67

Joslyn, H.D. and Dring, R.P., 1983, "Turbine Rotor Negative Incidence Stall", ASME Paper 83-GT-23

Leylek, J.H. and Zerkle, R.D., 1993, "Discrete-Jet Film Cooling: A Comparison of Computational Results with Experiments", ASME Paper 93-GT-207

Pedersen, D.R., Eckert, E.R.G., and Goldstein, R.J., 1977, "Film Cooling With Large Density Differences Between the Mainstream and the Secondary Fluid Measured by the Heat-Mass Transfer Analogy", ASME *Journal of Heat Transfer*, Vol. 99, pp. 620-627

Schmidt, D.L., Sen, B., and Bogard, D.G., 1994, "Film Cooling with Compound Angle Holes: Adiabatic Effectiveness", ASME Paper 94-GT-312

Shadid, J.N. and Eckert, E.R.G., 1991, "The Mass Transfer Analogy to Heat Transfer in Fluids with Temperature-Dependent Properties", ASME *Journal of Turbomachinery*, Vol. 113, pp. 27-33

Sieverding, C.H., 1984, "Recent Progress in the Understanding of Basic Aspects of Secondary Flows in Turbine Blade Passages", ASME *Journal of Engineering for Gas Turbines and Power*, Vol. 107, pp. 248-257

Sieverding, C.H. and Wilputte, P., 1980, "Influence of Mach Number and Endwall Cooling on Secondary Flows in a Straight Nozzle Cascade", ASME Paper 80-GT-52

Sinha, A.K., Bogard, D.G., and Crawford, M.E., 1991, "Film-Cooling Effectiveness Downstream of a Single Row of Holes with Variable Density Ratio", ASME *Journal of Turbomachinery*, Vol. 113, pp. 442-449

Soechting, F.O., Landis, K.K., and Dobrowolski, R., 1987, "Development of Low-Cost Test Techniques for Advancing Film Cooling Technology", AIAA-87-1913

Takeishi, K., Matsuura, M., Aoki, S., and Sato,T., 1989, "An Experimental Study of Heat Transfer and Film Cooling on Low Aspect Ratio Turbine Nozzles", ASME Paper 89-GT-187